



HAL
open science

Thermal tempering simulation of glass plates: Inner and edge residual stresses

Laurent Daudeville, Hélène Carré

► **To cite this version:**

Laurent Daudeville, Hélène Carré. Thermal tempering simulation of glass plates: Inner and edge residual stresses. *Journal of Thermal Stresses*, 1998, 21 (6), pp.667-689. 10.1080/01495739808956168 . hal-02004512

HAL Id: hal-02004512

<https://hal.science/hal-02004512>

Submitted on 13 Feb 2024

HAL is a multi-disciplinary open access archive for the deposit and dissemination of scientific research documents, whether they are published or not. The documents may come from teaching and research institutions in France or abroad, or from public or private research centers.

L'archive ouverte pluridisciplinaire **HAL**, est destinée au dépôt et à la diffusion de documents scientifiques de niveau recherche, publiés ou non, émanant des établissements d'enseignement et de recherche français ou étrangers, des laboratoires publics ou privés.

THERMAL TEMPERING SIMULATION OF GLASS PLATES: INNER AND EDGE RESIDUAL STRESSES

Laurent Daudville

Laboratoire de Mécanique et Technologie
Ecole Normale Supérieure de Cachan
CNRS, Univ. Paris 6
Cachan, France

Hélène Carré

Centre Scientifique et Technique du Bâtiment
Champs-sur-Mame, France

Narayanaswamy's model is used to describe the thermomechanical behavior of glass. It includes both stress relaxation (to take into account the viscous aspect of glass) and structural relaxation (to take into account the structure state of glass). The necessary thermal and mechanical characteristics are given for the float soda-lime silicate glass.

The thermal tempering of thin glass plates is simulated. Transient and residual stresses are given for the inner part of the plate. Computational results are compared with experimental results of previous works. This comparison validates Narayanaswamy's model associated with material characteristics given previously.

The edge effect (variation of stresses close to the edges) is described for thin plates. The thermal tempering of thick plates is simulated, and computational results are validated with optical measurements and a fractographic analysis.

The objective of this work is to provide a reliable computational method for the simulation of the thermal tempering of soda-lime silicate glass plates. Quenching consists of heating glass to a temperature above 600°C and cooling it brutally by air casts. Such thermal treatment induces residual stresses in the plate at the end of the cooling, thereby increasing the mechanical strength of glass parts.

In previous works, the simulation of an infinite glass plate has been carried out experimentally and numerically. Both inner and edge effects are analyzed in this article. The knowledge of residual stresses in the vicinity of edges is very important in the case of elements loaded in their plane. The main application of these glass components concerns building structures (beams or columns).

Glass is described as a viscoelastic material. Its behavior varies with time and temperature. Narayanaswamy's model, which includes both stress and structural relaxation (influence of the state of the glass structure), is used in this work.

The tridimensional residual stress state is computed using the *finite element method* (FEM). First, the model is checked by comparing the residual stresses in the inner part of thin plates from simulations and literature. The authors found it

difficult to obtain reliable data for the concerned material. No material datum was identified, and a sensitivity analysis to material parameters was conducted.

Then, the analysis of transient and residual stresses in the neighboring edges of tempered glass plates is presented. Inner and edge residual stresses were measured optically on several tempered glass plates. The heat transfer coefficients are temper process parameters. A comparison of two optical measurements with simulation results facilitates the identification of a priori unknown heat transfer coefficients.

The tempered glass plates were tested up to failure. A fractographic analysis gives the residual stress on the plate edge that cannot be measured optically.

The edge effect analysis is validated by a comparison of computed stresses with fractographic and optical information.

THERMOMECHANICAL MODELING OF GLASS

Generalized Maxwell's Model

For a tridimensional solicitation, the stress response ($\sigma(t)$) of a viscoelastic material can be separated into its volume and deviatoric parts:

$$\begin{cases} s_{ij}(x, t) = \int_{-\infty}^t G(t-t') \frac{\partial}{\partial t'} e_{ij}(x, t') dt' \\ \bar{\sigma}(x, t) = \int_{-\infty}^t K(t-t') \frac{\partial}{\partial t'} \bar{\epsilon}(x, t') dt' \end{cases} \quad (1)$$

where $\sigma_{ij} = s_{ij} + \bar{\sigma}\delta_{ij}$, $\epsilon_{ij} = e_{ij} + \bar{\epsilon}\delta_{ij}$, G = relaxation shear modulus, and K = relaxation bulk modulus. The generalized Maxwell's model is a rheological discrete model. It is an association of several Maxwell's models (spring and dashpot in series). The proposed rheological model of glass is illustrated in Figures 1 and 2 for

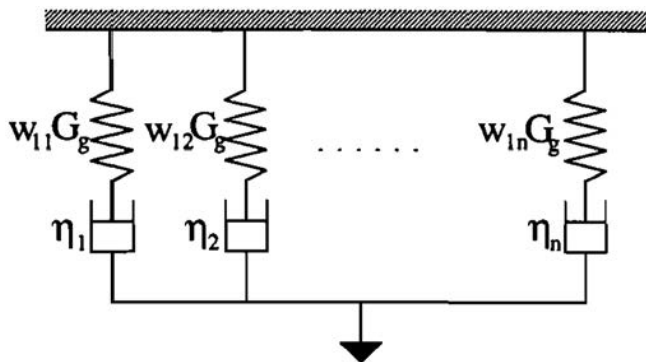


Figure 1. Generalized Maxwell's model for the deviatoric part.

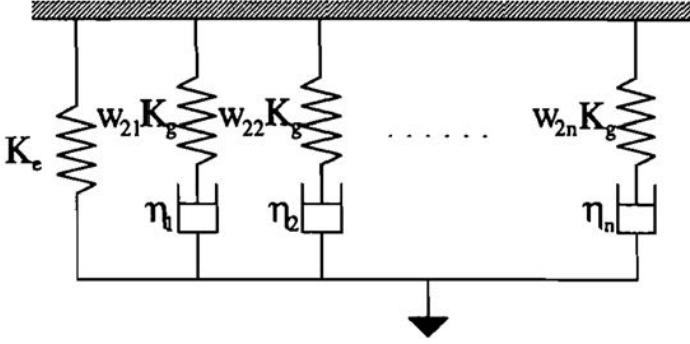


Figure 2. Generalized Maxwell's model for the volume part.

the deviatoric and volume parts, respectively [1, 2]. Relaxation shear and bulk moduli are described with instantaneous and deferred moduli and Prony's series.

For the deviatoric part

$$G(t) = 2G_g\Psi_1(t) \quad (2)$$

where

$$\Psi_1(t) = \sum_{i=1}^{n_1} w_{1i} \exp\left(-\frac{t}{\tau_{1i}}\right) \quad \tau_{1i} = \frac{\eta_i}{w_{1i}G_g}$$

G_g = instantaneous shear modulus, and G_e = deferred shear modulus = 0.

For the volume part

$$K(t) = 3K_e - (3K_e - 3K_g)\Psi_2(t) \quad (3)$$

where

$$\Psi_2(t) = \sum_{i=1}^{n_2} w_{2i} \exp\left(-\frac{t}{\tau_{2i}}\right) \quad \tau_{2i} = \frac{\eta_i}{w_{2i}K_g}$$

K_g = instantaneous bulk modulus, and K_e = deferred bulk modulus.

Stabilized Glass

When its structure is stabilized, glass can be considered a thermorheologically simple material. It means that the mechanical behavior is the same for different temperatures; only the rate of microstructural mechanisms changes. The relaxation function can be determined at any temperature if it is known at the reference temperature (T_{ref}). It consists of a shift of the relaxation function in a time logarithm scale [3].

The influence of the actual temperature T can be introduced by means of reduced time (ξ), which is defined as

$$\Psi_{i_r}(t) = \Psi_{i_{r_{ref}}}(\xi) \quad i = 1, 2 \quad (4)$$

Weights w_{1i} and w_{2i} , defined in $G(t)$ and $K(t)$, are constant with temperature. An Arrhenius relation allows a correct description of the times of relaxation changes with temperature [4, 5]:

$$\xi(t, T) = \int_0^t \frac{\tau_{ref}}{\tau(T, t')} dt' = \int_0^t \Phi(T(t)) dt' \quad (5)$$

where

$$\ln(\Phi(T)) = -\frac{H}{R} \left(\frac{1}{T_{ref}} - \frac{1}{T} \right)$$

H = energy of activation, and R = perfect gas constant.

Structural Relaxation

Quenching is a brutal thermal treatment. During cooling, the glass structure may not be stabilized. Since glass is sensible to the thermal loading rate, the structure state must be taken into account. That is Narayanaswamy's model [4, 6, 7].

The influence of the thermal loading rate can be shown by varying the specific volume with temperature (Figure 3). That phenomenon essentially concerns temperatures close to the transition range between the "glass" and "liquid" states.

Specific volume

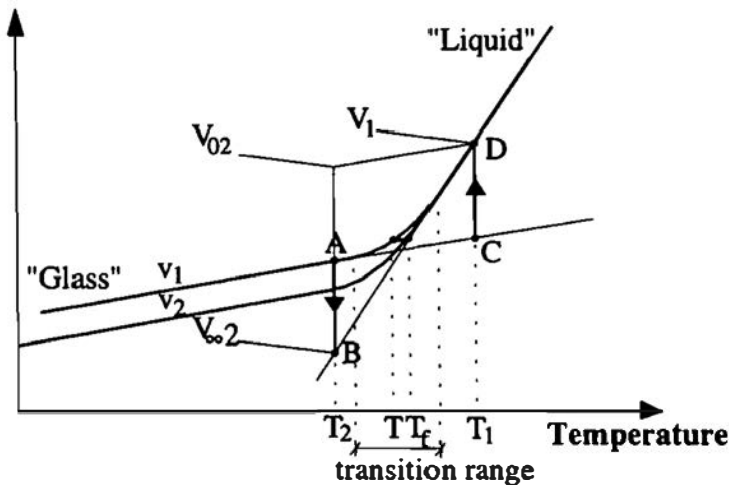


Figure 3. Variations of specific volume with temperature for two cooling rates.

When glass is heated to a temperature T_2 (point A on Figure 3) below the transition range, the structure of glass evolves to a stable state characteristic of the liquid glass (point B). This evolution is the direct structural relaxation. If the temperature is far below the transformation range, this evolution is too slow to be visible.

If glass is heated brutally to T_1 above T_g , the glass state goes to a point below the “liquid” straight line (point C). This unstable configuration changes to a stable one; the “liquid” glass state (point D). This process is called reverse structural relaxation.

There are several possible structural glass states for the same temperature depending on the cooling rate.

In 1946, Tool [8] introduced the fictive temperature (T_f) to take into account the structure of glass. Variations of the specific volume with temperature are used to describe variations of T_f .

- $T_f = T$ if T is above the transition range.
- T_f = the intersection between the “liquid” straight line and the parallel to the “glass” straight line in the transition range.
- T_f = the intersection between the “liquid” straight line and the “glass” straight line below the transition range.

A response function (M_v) is defined by varying the specific volume with temperature as

$$M_v(t) = \frac{V(t) - V_{\infty,2}}{V_{0,2} - V_{\infty,2}} = \frac{T_f - T_2}{T_1 - T_2} \quad (6)$$

where $T_1 - T_2$ = step of temperature, T_f = fictive temperature at T_2 , V = instantaneous specific volume, $V_{0,2}$ = volume just after the temperature change, and $V_{\infty,2}$ = equilibrium volume at T_2 .

The dependence of the response function on temperature is given by reduced time ξ . $M_v(t)$ can be considered the volume relaxation function and can define variations of the fictive temperature

$$T_f(t) = T(t) - \int_0^t M_v[\xi(t) - \xi(t')] \frac{dT(t')}{dt'} dt' \quad (7)$$

By analogy with viscous relaxation, the response function can be described with a Prony's series as

$$M_v(\xi) = \sum_{i=1}^n C_i \exp\left(-\frac{\xi}{\lambda_i}\right) \quad (8)$$

The fictive temperature variations are calculated with Markovsky and Soules' algorithm [9, 10]

$$T_f(t) = \frac{T_f(t - \Delta t) + T(t) \frac{\Delta t}{\lambda_i}}{1 + \frac{\Delta t}{\lambda_i}}$$

$$\lambda_i = \lambda_{i \text{ ref}} \exp \left\{ -\frac{H}{R} \left[\frac{1}{T_{\text{ref}}} - \frac{x}{T(t)} - \frac{1-x}{T_f(t - \Delta t)} \right] \right\} \quad (9)$$

$$T_f(t) = \sum_{i=1}^n C_i T_{f_i}(t)$$

$$T_f(0) = T_0$$

Structural relaxation times (λ_i) are considered proportional to shear relaxation times. A dilatometric curve facilitates obtaining their ratio, which has been found to be very close to 9 [11].

The fictive temperature allows one to take into account the structure state of glass. All characteristics vary with the actual temperature but also with the fictive temperature. The fictive temperature is introduced in the reduced time expression for the variations of viscoelastic characteristics by modifying Eq. 5

$$\xi(t, T, T_f) = \int_0^t \frac{\tau_{\text{ref}}}{\tau(T, t')} dt' = \int_0^t a(T(t), T_f(t)) dt' \quad (10)$$

where

$$\ln(a(T, T_f)) = -\frac{H}{R} \left(\frac{1}{T_{\text{ref}}} - \frac{x}{T} - \frac{1-x}{T_f} \right)$$

$x = \text{constant}$ ($0 < x < 1$), $H = \text{energy of activation}$, and $R = \text{perfect gas constant}$.

Introduction of Fictive Temperature

The dependency of viscosity on the structure state induces very small variations in residual stresses. But, the dependency of the density on the structure state has a much more significant effect on residual stresses (Figure 4).

Variations of viscosity in relation to the fictive temperature are not considered in our simulations. The influence of the structural state on the density is introduced by varying the thermal expansion coefficient in relation to temperature

$$\begin{aligned} \epsilon_{i,h} &= \beta_g(T(t) - T_f(t)) + \beta_l(T_f(t) - T_0) \\ &= \beta(t)(T(t) - T_0) \end{aligned} \quad (11)$$

Tension at the inner part (nm / c)

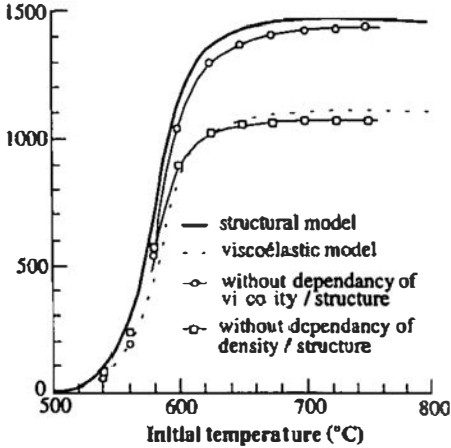


Figure 4. Influence of the fictive temperature on residual stresses [5].

where β_2 = thermal expansion coefficient of solid glass, β_1 = thermal expansion coefficient of liquid glass, T_0 = initial temperature, and β = equivalent thermal expansion coefficient.

FINITE ELEMENT MODELING

The thermal tempering of glass consists of using air casts to cool very rapidly the plate that was previously heated.

The problem that must be solved is time dependent. At each moment in time, the temperature is computed; then the nonlinear mechanical problem is solved. The nonlinear aspect is due to the viscous feature of the glass behavior.

The temperature of the glass plate is assumed to be uniform at the beginning of the computation (at a temperature above 600°C). In fact, the surface temperature of the glass plate decreases between the time it is removed from the oven and the beginning of cooling.

Heat Exchange Boundary Conditions

The cooling is modeled by a forced convection to each face of the plate. It is characterized by a heat transfer coefficient (h) and air temperature (T_{ext}). For a glass plate, three planes of symmetry and three forced convections define the cooling (Figure 5).

The exchange boundary condition by forced convection is written as

$$q = h(T_S - T_{ext}) \quad (12)$$

where q = heat flow, h = thermal transfer coefficient, T_S = surface temperature, and T_{ext} = room temperature.

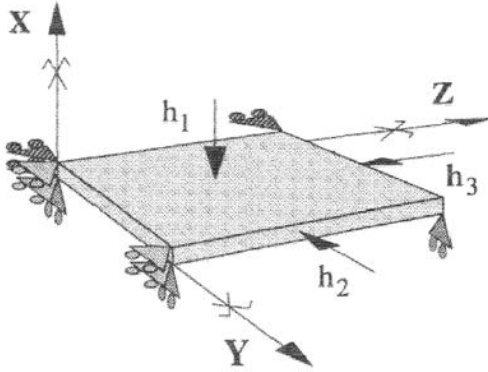


Figure 5. Displacement boundary conditions.

Radiation is accounted for in forced convection via the thermal transfer coefficient. The radiation boundary condition can be written as (by equivalence with convection)

$$\begin{aligned}
 q &= \sigma_{SB} e (T_S^4 - T_{ext}^4) \\
 &= \sigma_{SB} e (T_S^3 + T_S^2 T_{ext} + T_S T_{ext}^2 + T_{ext}^3) (T_S - T_{ext}) \\
 &= h_{eq} (\sigma_{SB}, e, T_S, T_{ext}) (T_S - T_{ext})
 \end{aligned} \tag{13}$$

where q = heat flow, σ_{SB} = Stefan-Boltzmann's coefficient, e = emissivity, T_S = surface temperature, T_{ext} = room temperature, and $h_{eq}(\sigma_{SB}, e, T_S, T_{ext})$ = equivalent thermal transfer coefficient. Thermal transfer coefficients are assumed to be constant during tempering.

Mesh and Displacement Boundary Conditions

Interesting results are the stress state in the middle of the plate and in the current part of the edges. The problem that needs to be solved does not depend on z because the plate is considered infinite in this direction. This is a plane problem since it depends only on x and y . Nevertheless, tridimensional elements are used to account for thermal deformation along z .

The modeling of an infinite strip implies quite complicated boundary conditions. Then, the tempering of an eighth of plate is simulated with the finite element code MARC. The mesh is refined in zones where stresses present high variations—in the thickness of the plate (along x) and close to the edge (along y).

The edge effect is not studied along z because it is similar to that along y . The displacement boundary conditions that are introduced are symmetry conditions; that is, there is no displacement perpendicular to the plane of symmetry (Figure 5).

Glass Characteristics

Glass is a very old material that has been studied for a long time. But mechanical and thermal characteristics are not well known because they depend on the glass

composition and are difficult to measure experimentally (in particular, for the viscoelastic characteristics and the thermal expansion coefficient of the liquid glass).

The six mechanical characteristics of Narayanaswamy's model that are used in simulations are as follows.

- *Elastic characteristics* at room temperature [1]

$$\begin{aligned} \text{Young modulus} & E = 7.10^{10} \text{ Pa} \\ \text{Poisson ratio} & \nu = 0.22 \end{aligned}$$

- *Viscoelastic characteristics* [1] (Table 1),
- *Structural characteristics* for the calculation of T_f [12] (Table 2).

The energy of activation is not a well-known parameter. The dependence of glass viscosity on temperature was determined in a previous work [1]. It is an empirical relation of Vogel–Fulcher–Tammann

$$\begin{aligned} \text{Log}(\eta) &= A + \frac{B}{T - T_0} \\ &= -1.993 + \frac{4003.5}{T - 542} \quad \text{for } T > T_g \quad \text{where } \eta = (\tau_1)G \end{aligned} \quad (14)$$

The value of the ratio H/R was identified by comparing the previous relation with the function $\Phi(T)$ of Narayanaswamy's model

$$H/R = 55,000 \text{ K}$$

- *Thermal expansion coefficient* [12]

$$\begin{aligned} \text{solid glass (room temperature)} & \beta_g = 9.10^{-6} \text{ } ^\circ\text{C}^{-1} \\ \text{liquid glass (high temperature)} & \beta_l = 25.10^{-6} \text{ } ^\circ\text{C}^{-1} \end{aligned}$$

Table 1 Characteristics of shear and volume moduli

Deviatoric part ($T_{ref} = 859 \text{ K}$)		Volume part ($K_r/K_g = 0.18$) ($T_{ref} = 869 \text{ K}$)	
G_i (10^9 Pa)	τ_{1i} (s)	K_i (10^9 Pa)	τ_{2i} (s)
1.5845	$6.658 \cdot 10^{-5}$	0.7588	$5.009 \cdot 10^{-5}$
2.3539	$1.197 \cdot 10^{-3}$	0.7650	$9.945 \cdot 10^{-4}$
3.4857	$1.514 \cdot 10^{-2}$	0.9806	$2.022 \cdot 10^{-3}$
6.5582	$1.672 \cdot 10^{-1}$	7.301	$1.925 \cdot 10^{-2}$
8.2049	$7.497 \cdot 10^{-1}$	13.47	$1.199 \cdot 10^{-1}$
6.4980	3.292	10.896	2.033

Table 2 Characteristics of the response function for the structural part

Structural part	
C_i	$\lambda_i(s)$
$5.523 \cdot 10^{-2}$	$5.965 \cdot 10^{-4}$
$8.205 \cdot 10^{-2}$	$1.077 \cdot 10^{-2}$
$1.215 \cdot 10^{-1}$	$1.362 \cdot 10^{-1}$
$2.286 \cdot 10^{-1}$	1.505
$2.860 \cdot 10^{-1}$	6.747
$2.265 \cdot 10^{-1}$	29.63

The thermal conductivity and the specific heat are the thermal characteristics. They vary with temperature [12].

- Thermal conductivity (W/m.K)

$$\lambda = 0,975 + 8,58 \cdot 10^{-4} T \quad \text{where } T \text{ in } ^\circ\text{C}$$

- Specific heat (J/kg.K) [11] (with T in K)

$$\text{liquid glass } (T > T_g = 850 \text{ K}) \quad C_{p,l} = 1433 + 6.5 \cdot 10^{-3} T$$

$$\text{solid glass } (T < T_g) \quad C_{p,s} = 893 + 0.4T - 1.8 \cdot 10^{-7} / T^2$$

INNER EFFECT

Experimental studies give the residual stress state in the inner part of thin plates (0.61-cm thick) [4, 6]. The tempering simulation of these glass plates is presented and compared to previous works for the validation of the model [13, 14].

Results

During tempering, the temperature decreases more rapidly at the surface than in the inner part (Figure 6). A thermal gradient appears in the thickness (which can be greater than 150°C); it implies transient and residual stresses.

At the beginning of cooling, the surface contracts more rapidly than the inner part, which leads to a compression state at the core and a tensile state at the surface by equilibrium. The transient tensile stress on the surface can induce failure at the onset of cooling.

When the surface temperature is below the transition range, the surface congeals. The core, still liquid, continues to cool and contract. The surface is then in compression and the core in tension. After several tens of seconds, stresses are stabilized (Figure 7).

In the middle of the plate, the residual tractions are equal for directions y and z . Stresses are parabolic in the thickness. The surface compressive stress is twice

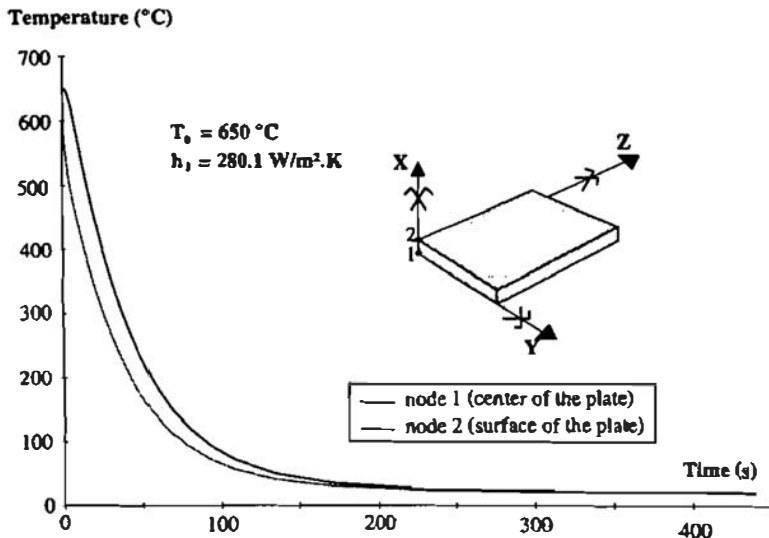


Figure 6. Variations of temperature with time.

higher than the tensile midplane stress (Figure 8). This stress state gives plates a better mechanical strength.

The characteristic parameter values of the model were obtained from different works. A large discrepancy in the values can be observed in the literature, possibly due to the difficulty involved in measuring some characteristics and to sensibility to the glass chemical composition.

In order to study the influence of characteristic parameter values, a sensibility analysis is carried out by varying the mechanical and thermal parameters: Young's modulus (E), the Poisson ratio (ν), the solid and liquid glass thermal expansion coefficients (β_g and β_l), reference temperature (T_{ref}), specific heat (C_p), and thermal conductivity (λ). The parameters are modified (+20%, +10%, -10%, -20%) from a current case: $T_0 = 650^\circ\text{C}$ and $h_1 = 280.1 \text{ W/m}^2.\text{K}$.

Variations of residual stresses in the surface and in the midplane are observed. The Poisson ratio, the solid glass thermal expansion coefficient, the specific heat, and the thermal conductivity are parameters of less importance than the others. The variations of the residual stresses are quasi-proportional to the variations of Young's modulus and of the liquid glass expansion thermal coefficient. The reference temperature is a parameter of great importance because it controls the viscoelastic behavior (Figures 9 and 10).

Comparisons with Experimental Works

Experimental results issued from [4, 6] are compared with FEM results obtained with the previous glass characteristics.

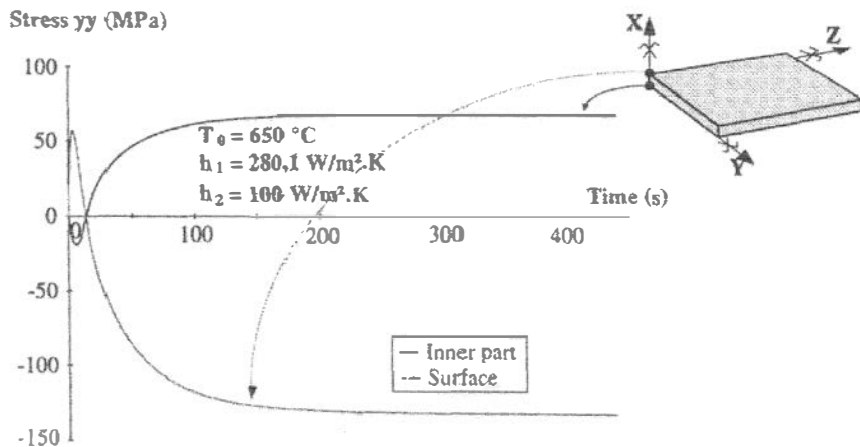


Figure 7. Variations of stress with time.

The variation of the traction (σ_{yy}) in the thickness is compared with optical measurements from [6] in a particular case of quenching ($T_0 = 738^\circ\text{C}$ and $h_1 = 221.5 \text{ W/m}^2\cdot\text{K}$) (Figure 11).

In Figure 12, experimental [5] and numerical results are given. They show the influence of the cooling rate (h) and the initial temperature (T_0) on the residual tensile stress in the core of the plate. The higher h , the higher this residual traction. They also reveal a dependence on the initial temperature: the residual

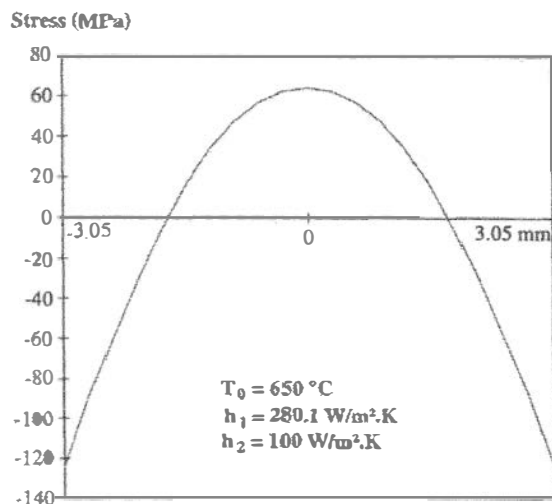


Figure 8. Residual stress in the thickness of the plate.

Residual stress in middle plane

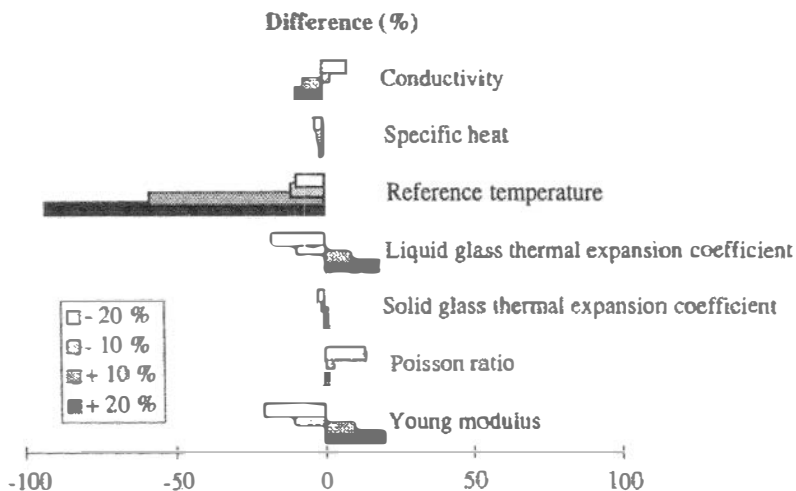


Figure 9. Sensibility analysis for residual stress in the middle plane.

Residual stress in surface

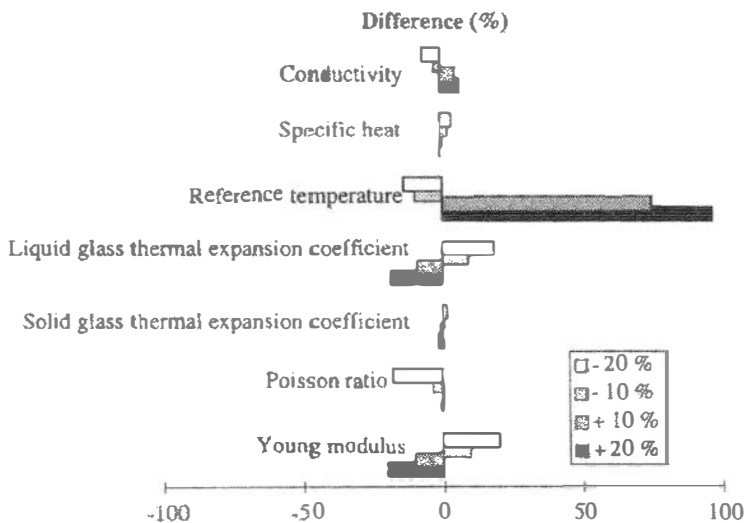


Figure 10. Sensibility analysis for residual stress in the surface.

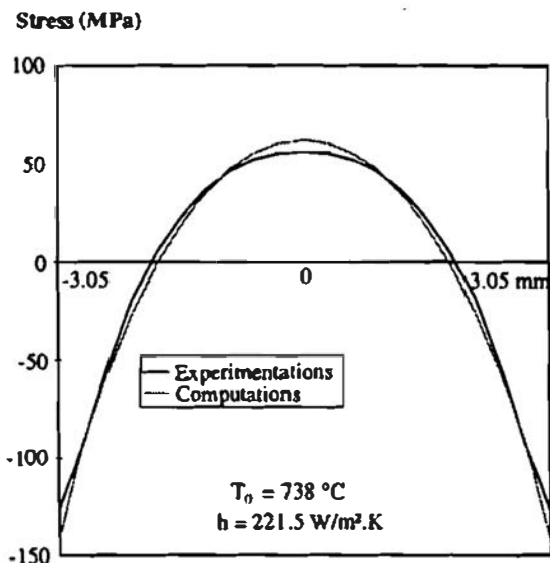


Figure 11. Variation of stress in the thickness.

stress increases with the initial temperature until 680°C, where it becomes quasi-constant with T_0 .

This satisfying comparison between computational and experimental results validates Narayanaswamy's model given the chosen data.

EDGE EFFECT

The goal is the determination of tridimensional transient and residual stresses on the edge of glass plates where fracture may occur. The inner effect of tempering was presented for thin plates. The edge effect is now studied, on one hand, to the same thin plates and, on another hand, to thick plates (19-mm thickness) for a comparison with optical measurements.

The tempering parameters are the initial temperature (easily determined during the industrial process) and the thermal transfer coefficients (unknown). Thermal transfer coefficients can be calculated by an inverse analysis.

Results

As for the inner effect, the stress sign changes during tempering on the edges. The transient traction (σ_{yy}) is very high at the corner (point 4). At the end of the cooling phase, the three points on the surface (points 2, 3, 4) are in compression even though the core is in tension (point 1) (Figure 13).

In the middle of the plate, the stresses are parabolic along the thickness (Figure 14). The stress profile in the thickness on the edge depends on the ratio

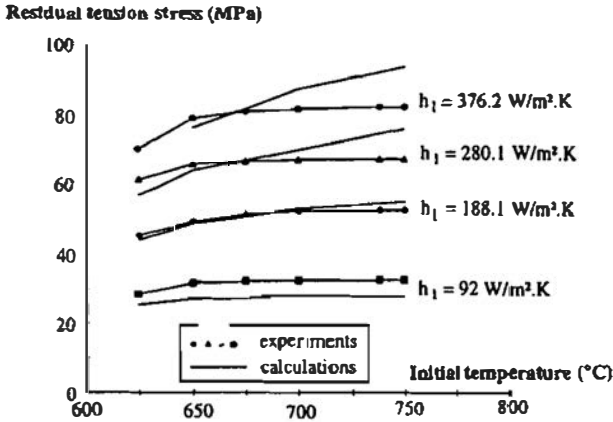


Figure 12. Variations of residual tension stress with quenching parameters.

h_1/h_2 , where h_1 is the thermal transfer coefficient of convection on the plane and h_2 is the thermal transfer coefficient on the edge (Figure 5). If h_2 is below h_1 , the traction along z (σ_{zz}) is more important at the corner than in the middle of the edge. If h_2 is far above h_1 , it is the contrary.

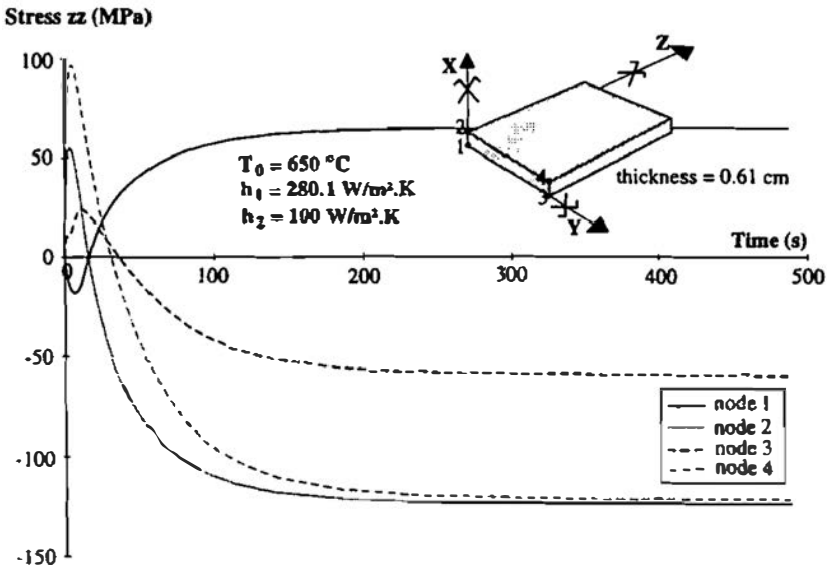


Figure 13. Variations of stress σ_{zz} with time in the inner part and at the edge.

Stress σ_x (MPa)

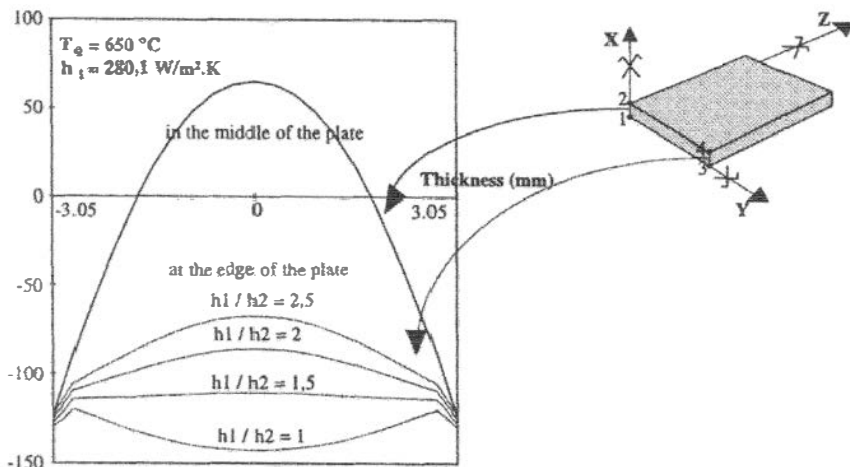


Figure 14. Variation of stress σ_{xx} in the thickness in the middle and at the edge for several values of h_2 .

Influence of the Chamfer

The chamfer introduced for the computations of thin glass plates is 0.5-mm wide. The thermal transfer coefficient is assumed to be the same in the broken corner as in the edge. The chamfer has no influence on the residual stresses (Figure 15) but can decrease the value of the maximum transient surface tension stress (Figure 16).

Case of a Thick Plate

Optical measurements. Tempered glass is birefringent. The photoelasticimetry technology allows stress measurements [15]. Two kinds of these measurements are realized on thick tempered glass plates.

First, the Epibiascope [16, 17] is an apparatus that is used to obtain the surface stress. It is measured in several points in the inner part of the plate ($\sigma_{yy} = \sigma_{zz}$)

$$\text{mean} = 120,4 \text{ MPa}$$

$$\text{standard deviation} = 4,9 \text{ MPa}$$

$$\text{with precision of measurement} = \pm 6 \text{ MPa}$$

The Babinet compensator measures the difference of the optical path in the thickness of the plate, which is proportional to the integral in the thickness of the difference of principal stresses ($\bar{\sigma}_{yy} - \bar{\sigma}_{zz}$) [18]. This integral is equal to zero in the middle of the plate. The measurements are done close to the edge (1.5 mm from

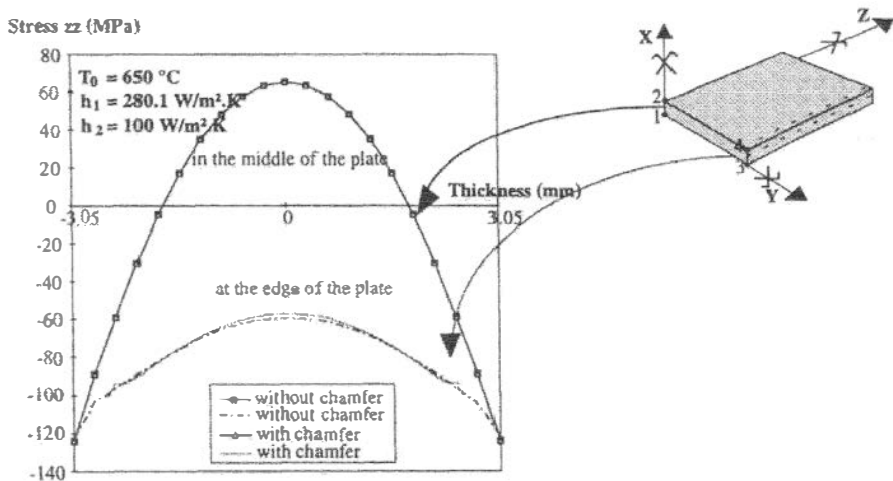


Figure 15. Stress σ_{zz} in the thickness in the middle and at the edge of the plate with and without chamfer.

the edge), at the limit of the chamfer:

mean = 72,0 MPa

standard deviation = 3,3 MPa

with precision of measure = $\pm 1,2$ MPa

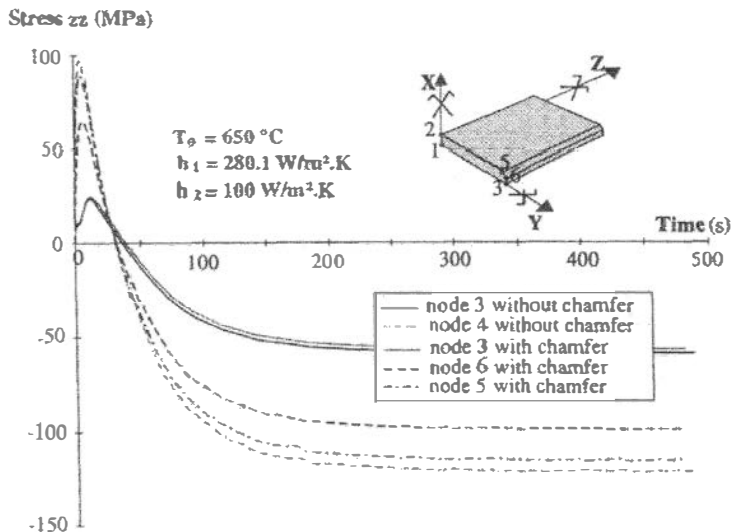


Figure 16. Variations of stress σ_{zz} with time in the middle and at the edge with and without chamfer.

Several measures at different distances from the edge were carried out. The variations of the integral in the thickness of the difference of principal stresses with the distance from the edge are given (Figure 17).

Results.

Determination of thermal transfer coefficients Uniform tempering of a glass plate is characterized by four parameters:

T_0 = initial temperature

h_1 = thermal transfer coefficient of convection on the plane

h_2 = thermal transfer coefficient of convection on the edge

T_{ext} = temperature of blown air

The initial temperature and the temperature of blown air can be determined quite easily during the industrial process. For studied thick plates, their values are 620°C and 20°C, respectively. h_1 and h_2 are very difficult to measure. These coefficients will be identified by a comparison of optical measurements with calculation results. Since the surface residual stress values in the inner part of the plate are only governed by h_1 , the Epibiascope measurements allow one to determine h_1

$$h_1 = 135 \text{ W/m}^2.\text{K}$$

The edge stresses are controlled by both h_1 and h_2 . h_2 can be identified with the Babinet compensator measurement at the limit of the chamfer (point A on Figure 17)

$$h_2 = 115 \text{ W/m}^2.\text{K}$$

Validation of simulations.

Validation by optical measurements In Figure 17, only one point was used to determine the thermal transfer coefficient h_2 . Figure 18 shows a comparison of optical measurements and computational results from the edge to the inner part.

Validation by fractographic analysis Thick tempered glass plates were tested to failure under four-point bending. The local failure stress is obtained with the ultimate load using beam theory.

A semicircular shiny zone (mirror of failure) can be observed in the failure pattern of annealed glass. The mirror radius, corresponding to a *crack branching*

Integral of the difference of principal stresses (MPa)

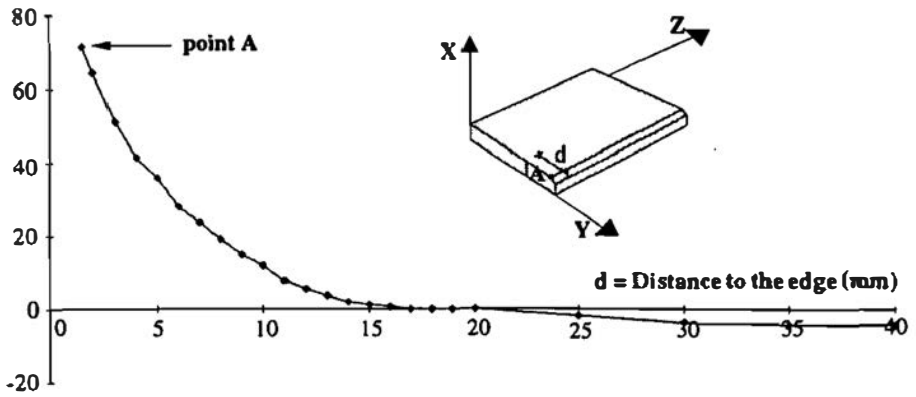


Figure 17. Variations of the integral of the difference of principal stresses with the distance from the edge.

Integral of the difference of principal stresses (MPa)

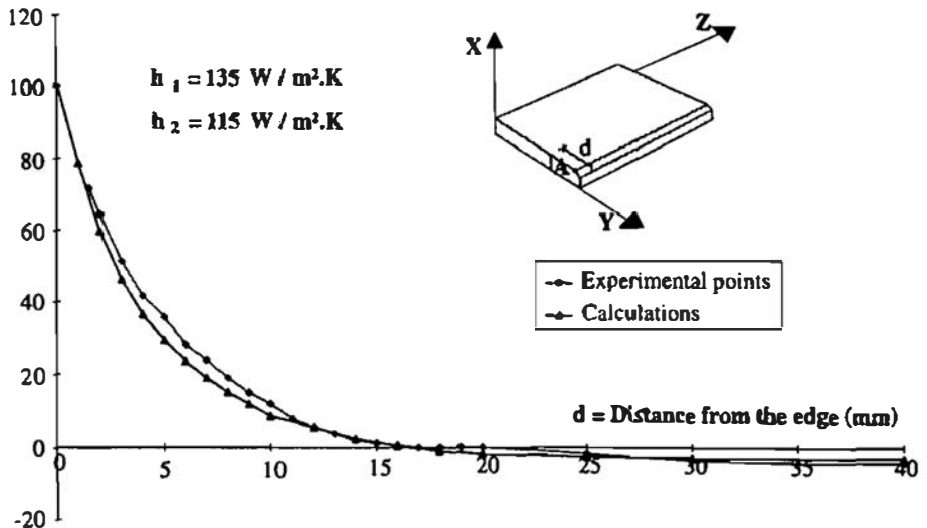


Figure 18. Variations of the integral of the difference of principal stresses with the distance from the edge.

(CB), can be linked to the tensile failure stress by [19]

$$\sigma_{\text{failure}} = \frac{M}{\sqrt{r_m}} \quad (15)$$

where r_m = mirror radius and $M = 1.85 \text{ MPa}\cdot\text{m}^{1/2}$. The previous relation is obtained using linear elastic fracture mechanics theory.

For tempered glass, the failure mirror is also observed (Figure 19). The residual stress state must be taken into account in the fractographic analysis. The stress intensity factor can be written [20, 21] as

$$K_I = \frac{2}{\sqrt{\pi}} \sigma_A \sqrt{a} Y_F(\theta) - \frac{2}{\sqrt{\pi}} \sigma_R \sqrt{a} Y_R(\theta) \quad (16)$$

where a = crack radius, $Y_F(\theta)$ = shape factor associated with bending, and $Y_R(\theta)$ = shape factor associated with residual stress = 1. The apparent failure stress (σ_A), the residual compression stress (σ_R), and the mirror radius (r_m) can be linked ($K_I = K_{CB}$ and $a = r_m$) via

$$\sigma_A \sqrt{r_m} Y_F(\theta) = \sigma_R \sqrt{r_m} + \psi_0 \quad (17)$$

where $\psi_0 = 2.41 \text{ MPa}\cdot\text{m}^{1/2}$ and $Y_F(\theta) = K_{CB}/M = 2.33/1.85 = 1.26$. Measurements were taken for two plates:

$$\text{radius 1} = 2.5 \text{ mm} \quad \sigma_{A1} = 118.6 \text{ MPa} \quad \sigma_R = 101.2 \text{ MPa}$$

$$\text{radius 2} = 1.19 \text{ mm} \quad \sigma_{A2} = 135.1 \text{ MPa} \quad \sigma_R = 100.4 \text{ MPa}$$

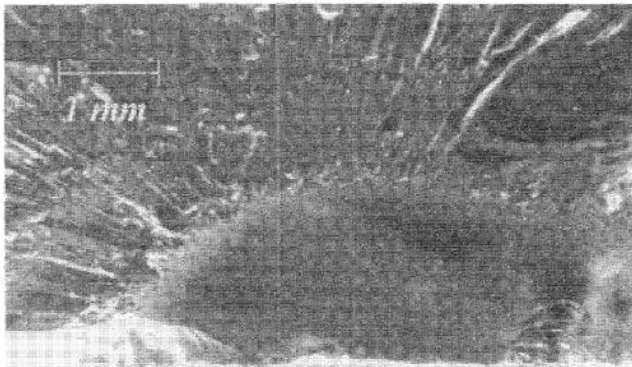


Figure 19. View of failure mirror of a thick tempered glass plate.

These values of residual stresses must be compared to the mean value of the compression stress on the edge obtained with calculations: 101.1 MPa (maximum = 108.8 MPa and minimum = 93.8 MPa). The deviation is only about 1%.

Residual stresses. The residual stresses in the inner part of the plate are parabolic along the thickness, as seen earlier for thin plates. The residual stress value on the edge of the plate is quasi-constant and slightly inferior to the surface residual stress in the inner part of the plate (Figure 20).

CONCLUSION

The FEM of modeling glass tempering was presented. The calculation of the tridimensional residual stress state in the edge regions is necessary for a possible failure analysis. The use of Narayanaswamy's model to describe the glass thermo-mechanical behavior is validated thanks to comparisons between our calculated results and the experimental results of previous works. The sensibility analysis has shown the foreseeable importance of Young's modulus and the liquid glass thermal expansion coefficient values on the residual stress state. Among the other material parameters of our model, the reference temperature is the more sensitive. The

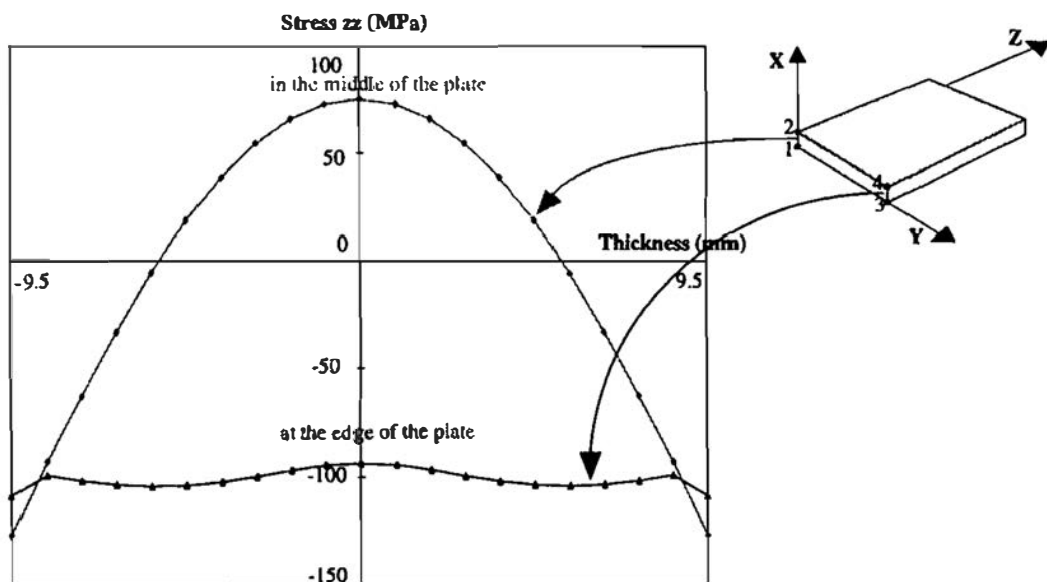


Figure 20. Variations of σ_{zz} in the middle and at the edge of the plate in the thickness.

glass behavior depends on the chemical glass composition, and a slight change in the reference temperature implies great changes in the residual stresses.

The edge effect can be analyzed using the variations of stresses close to the edges. The residual stress shape in the edge depends on the thermal transfer coefficient of forced convection applied in the edge. Two kinds of experiments are done to validate residual stress values close to the edge: optical measurements and fractographic analysis.

An experimental campaign was carried out to identify the fracture features of glass [22]. The lifetime of glass components in building structures can be analyzed with the presented approach.

REFERENCES

1. L. Duffrene, Comportement viscoélastique d'un verre silico-sodocalcique dans le domaine des températures intermédiaires, Thesis, École Nationale Supérieure des Mines de Paris, Paris, 1994.
2. R. Gy, L. Duffrene, and M. Labrot, New Insights into the Viscoelasticity of Glass, *J. Non-Crystalline Solids*, vol. 175, pp. 103–117, 1994.
3. F. Schwarzl and A. J. Staverman, Time-Temperature Dependence of Linear Viscoelastic Behavior, *J. Appl. Phys.*, vol. 23, no. 8, 1952.
4. O. S. Narayanaswamy, Stress and Structural Relaxation in Tempering Glass, *J. Amer. Ceramic Soc.*, vol. 61, no. 3–4, pp. 146–152, 1978.
5. R. Gardon, Thermal Tempering of Glass, in D. R. Uhlmann and N. J. Kreidl (eds.), *Glass: Science and Technology*, Academic Press, New York, 1980.
6. O. S. Narayanaswamy and R. Gardon, Calculation of Residual Stresses in Glass, *J. Amer. Ceramic Soc.*, vol. 52, no. 10, pp. 554–558, 1969.
7. O. S. Narayanaswamy, A Model of Structural Relaxation in Glass, *J. Amer. Ceramic Soc.*, vol. 54, no. 10, pp. 491–498, 1971.
8. A. Q. Tool, Relation Between Inelastic Deformability and Thermal Expansion of Glass in Its Annealing Range, *J. Amer. Ceramic Soc.*, vol. 29, no. 9, pp. 240–253, 1946.
9. A. Markovsky and T. F. Soules, An Efficient and Stable Algorithm for Calculating Fictive Temperatures, *J. Am. Ceram. Soc.*, vol. 67, no. 4, C-56-C-57, 1984.
10. M. A. Burke, T. F. Soules, R. F. Busbey, and S. M. Kheson, Finite-Element Calculation of Stresses in Glass Parts Undergoing Viscous Relaxation, *J. Amer. Ceramic Soc.*, vol. 70, no. 2, pp. 90–95, 1987.
11. C. Guillemet, R. Gy, and M. Labrot, Viscosity, Configurational Entropy and Structural Relaxation of Silica-Soda-Lime Glass, *Proc. XVIth Int. Congress in Glass*, Madrid, 1992.
12. Saint-Gobain Recherche, Private communication.
13. H. Carre and L. Daudeville, Finite Element Calculation of Stresses in Tempered Glass, *Proc. 1st Int. Sympos. Thermal Stresses and Related Topics*, Hamamatsu, Japan, 1995.
14. H. Carre and L. Daudeville, Numerical Simulation of Soda-Lime Silicate Glass Tempering, *Proc. J. Physique IV, Colloque C1, Suppl. J. Physique III*, vol. 6, pp. 175–185, 1996.
15. V. Novotny, Relation entre les contraintes au voisinage de la surface des verres trempés, déterminées à l'aide d'un épibioscop, leur degré de trempe et leur destruction après Casse, *Verres et réfractaires*, vol. 35, no. 5, 1981.
16. H. Aben and C. Guillemet. *Photoelasticity of Glass*. Springer-Verlag, Berlin, Germany, 1993.
17. A. S. Redner, How to Measure Stress in Glass, *Glass Digest*, 1994.
18. N. K. Sinha, Stress State in Tempered Glass Plate and Determination of Heat-Transfer Rate, *Experimental Mechanics*, vol. 18, no. 1, pp. 25–34, 1978.
19. J. C. Conway and J. J. Mecholsky, Use of Crack Branching Data for Measuring Near Surface Residual Stresses in Tempered Glass, *J. Amer. Ceramic Soc.*, vol. 72, no. 9, pp. 1584–1587, 1989.

20. E. B. Shand, Breaking Stress of Glass Determined from Dimensions of Fracture of Mirrors, *J. Amer. Ceramic Soc.*, vol. 42, no. 10, pp. 474-477, 1959.
21. M. J. Kerper and T. G. Scuderi, Relation of Strength of Thermally Tempered Glass to Fracture Mirrors Size, *Amer. Ceramic Soc. Bull.*, vol. 44, no. 12, pp. 953-955, 1965.
22. H. Carre, Détermination de la résistance du verre trempé pour son utilisation en génie civil, *Proc. 14ème Rencontres Universitaires de Génie Civil*, Clermont-Ferrand, 1996.